Modelling of localization and propagation of phase transformation in superelastic SMA by a gradient nonlocal approach

Arnaud Duval, Mohamed Haboussi, Tarak Ben Zineb

Modelling of localization and propagation of phase transformation in superelastic SMA by a gradient nonlocal approach

A. Duval, M. Haboussi, T. Ben Zineb

PII: S0020-7683(11)00086-2
DOI: 10.1016/j.ijsolstr.2011.02.019
Reference: SAS 7262

To appear in: *International Journal of Solids and Structures*

Received Date: 19 March 2010
Revised Date: 14 February 2011
Accepted Date: 22 February 2011

Please cite this article as: Duval, A., Haboussi, M., Ben Zineb, T., Modelling of localization and propagation of phase transformation in superelastic SMA by a gradient nonlocal approach, *International Journal of Solids and Structures* (2011), doi: 10.1016/j.ijsolstr.2011.02.019

Modelling of localization and propagation of phase transformation in superelastic SMA by a gradient nonlocal approach

A. Duval, M. Haboussi*, T. Ben Zineb

LEMTA, Nancy University, CNRS, 2 rue Jean Lamour, 54500, Vandoeuvre-lès-Nancy, France.

Abstract

In this work, a nonlocal phenomenological behavior model is proposed in order to describe the localization and propagation of stress-induced martensite transformation in Shape Memory Alloy (SMA) wires and thin films. It is a nonlocal extension of an existing local model that was derived from a micromechanical-inspired Gibbs free energy expression. The proposed model uses, besides the local field of the internal variable, namely the martensite volume fraction, a nonlocal counterpart. This latter acts as an additional degree of freedom, which is determined by solving an additional Partial Differential Equation (PDE), derived so as to be equivalent to the integral definition of a nonlocal quantity. This PDE involves an internal length parameter, dictating the global scale at which the nonlocal interactions of the underlying micromechanisms are manifested during phase transformation. Moreover, to account for the unstable softening behavior, the transformation yield force parameter is considered as a gradually decreasing function of the martensite fraction. Possible material and geometric imperfections that are responsible of localization initiation are also considered in this analysis. The obtained constitutive equations are implemented in the `Abaqus`®finite element code in one and two dimensions. This requires the development of specific finite elements having the nonlocal volume fraction variable as an additional degree of freedom. This implementation is achieved through the UEL user's subroutine. The effect of martensitic localization on the superelastic global behavior of SMA wire and holed thin plate, subjected to tension loading, is analyzed. Numerical results show that the developed tool correctly captures the commonly observed unstable superelastic behavior characterized by nucleation and propagation of martensitic phase. In particular, they show the influence of the internal length parameter, appearing in the nonlocal model, on the size of the localization area and the stress nucleation peak.

Key words: Shape Memory Alloy, Superelasticity, Nucleation, Softening,

*Corresponding author
Email address: `Mohamed.Haboussi@ensem.inpl-nancy.fr` (M. Haboussi)

Localization, Instability, Nonlocal gradient models, Finite Element

1. Introduction

The specific behavior of SMAs on the shape memory effect and pseudoelasticity at one hand and their high mechanical work/volume ratio on the other hand make them particularly well adapted for the design of microcomponents, (Reynaerts et al., 1997; Benard et al., 1998; Tabib-Azar et al., 1999; Kyung et al., 2008; Bellouard, 2008). An example of SMAs whose practical use is rapidly growing is the NiTi, due to its excellent structural properties. The development of finite element tool dedicated for the numerical design of any systems requires the modelling of the material behavior. In the case of small sized SMA samples such as wires and thin films, the material exhibits unstable softening behavior during stress-induced martensite phase transformation. This unstable behavior manifests itself by strain (martensite fraction) localization and propagation, characterized by a stress peak (nucleation) followed by a plateau (propagation). This Luders-like deformation has been shown in many experimental works since the one of (Shaw and Kyriakides, 1995) (See Fig. 1 for a schematic of this behavior). This particular behavior is the consequence of a material-level instability of the phase transformation at the microscale, it is also influenced by geometric factors such as wire thinning (Shaw and Kyriakides, 1997), the radius/length ratio in the case of a tube specimen (He and Sun, 2009a,b; Cai and Dai, 2006), or the width/length ratio for plate (He and Sun, 2010).

Various models are available in the literature, that is dedicated to the macroscopic description of the thermomechanical behavior of bulk SMAs. Among these models, we mention those reported in (Tanaka, 1986; Tanaka et al., 1995; Raniecki and Lexcellent, 1998; Bekker and Brinson, 1998; Thamburaja, 2005; Panico and Brinson, 2007; Popov and Lagoudas, 2007; Zaki and Moumni, 2007; Peultier et al., 2006; Saint-Sulpice et al., 2009; Arghavani et al., 2010). These models developed within a local context (based on the assumption of a uniform Representative Elementary Volume(REV)) fail to describe the aforementioned softening and localization phenomena. In fact, the material response predicted on the basis of such modelling will suffer from the pathological problem of mesh dependency which taints their prediction of a lack of objectivity. Moreover, such response will be singular as it localizes in a region of zero volume for very fine meshing. This type of pathological response was observed by (Shaw and Kyriakides, 1998; Azadi et al., 2007) during the simulation of stress-induced martensitic transformation by using a plasticity-inspired local theory. More recently, gradient-based nonlocal models have been proposed in order to describe such unstable behavior, without the singularity problem. As a matter of example, one can quote the contributions of (He and Sun, 2009a,b, 2010; Chang et al., 2006). In (He and Sun, 2009a,b), a gradient behavior macroscopic model of a NiTi polycristalline SMA is developed within the continuum

Ginzburg-Landau elastic framework. Based on a nonconvex strain energy density function completed by a strain gradient term, the model well describes the influence of structural and material lengths on the macroscopic strain domain formation and their evolution, in tube and thin plate during stress-induced phase transformation. The hysteresis effect of SMA material had not been considered yet. In (Chang et al., 2006), a thermodynamics-based 1D continuum model of SMA is proposed. It includes two internal variables (tensile and compression martensite phase fractions), possible unstable mechanical behavior, relevant thermomechanical couplings resulting from latent heat effects, and a regularizing strain gradient term, which is injected in an expression of the Helmholtz free energy potential. The model is used to study numerically the effects of displacement loading rate and environmental parameters on the shape memory effect and pseudoelastic behavior of polycrystalline NiTi wire.
Other types of models can be found in the literature, related to the topic of transformational unstable behavior description, which are less adapted to structural calculation, among them (Ahluwalia et al., 2004; Truskinovsky and Vainchtein, 2004; Sun and He, 2008). In (Ahluwalia et al., 2004), a micromechanical model based on the theory of Ginzburg-Landau is proposed in order to study the domain morphology, and mechanical properties of shape memory polycristals alloys in different temperature regimes. In (Truskinovsky and Vainchtein, 2004), a discrete model is proposed whose objective is the obtaining of specific relations between the macroscopic parameters of the stress peak, and the microscopic characteristics of the material. In (Sun and He, 2008), a multiscale gradient model is developed in order to describe the rapid decrease in stress hysteresis with grain size.
In this study, another nonlocal modelling approach of SMA unstable behavior is proposed. Implemented in a commercial finite element software (`Abaqus`®), the resulting model is used in the analysis of the pseudoelastic behavior of small sized structures (wire and holed thin plate). The specificity of such an approach is the obtaining of the nonlocal model as an extension of an existing local model that was derived from a micromechanical-inspired Gibbs free energy expression, (Peultier et al., 2006), and which proved its efficiency in describing SMA bulk behavior under a wide range of thermomechanical loading conditions. The proposed nonlocal extension is inspired from the work of (Peerlings et al., 2001) and (Engelen et al., 2003) on nonlocal continuum damage and plasticity respectively. It is a gradient-based enhancement of the local constitutive equations, performed so as to preserve a nonlocality of a strong type, i.e. with a long range interaction between the material point constitutive response and the remaining domain, in contrast to the conventional gradient approaches known as of a weak nonlocality type. Thus, limiting temporarily ourselves to the superelasticity framework, a nonlocal definition of the internal variable field, which is here the martensite volume fraction, is adopted besides the local counterpart. The nonlocal field acts as an additional degree of freedom, which is determined by solving an additional Partial Differential Equation (PDE). The latter is obtained as a Taylor's approximation of the integral definition of a nonlocal quantity. This PDE involves an internal length parameter that determines the global

scale at which the nonlocal interactions of the underlying micromechanisms are manifested during phase transformation. It is completed by ad hoc boundary conditions, stating that no evolution of the martensite fraction is assumed at the domain limit, and preserving the total amount of martensite between the local model and its nonlocal extension.
It is important to mention that the aforementioned nonlocal changes of the local model provide a localization limiter in presence of softening behavior. To consider this unstable softening behavior in the present approach, a local model ingredient, that is the yield transformation force, is modified as a gradually decreasing function of the martensite fraction, meaning that once the phase transformation starts, less energy is required to continue the transformation process, (Shaw and Kyriakides, 1997; Sun and He, 2008; Churchill et al., 2009). Furthermore, the localization of phase transformation is depicted by assuming the yield transformation force parameter as spatially non uniform (existence within the structure of a finite size area with smaller value of the yield force), accounting for the presence of a supposed material defect in the studied SMA wire. In the case of the studied SMA thin plate, the localization is assumed to be provoked by a geometrical "defect" materialized by a hole, instead of the material defect precedently evoked .
The obtained constitutive equations are numerically solved in a coupled fashion with the equilibrium equation of the 1D and 2D treated problems. This leads to the development of two specific finite elements having the nonlocal volume fraction variable as an additional degree of freedom. The implementation is achieved in `Abaqus`® finite element code through the UEL user's subroutine. The effect of martensitic localization on the superelastic global behavior of SMA wire and holed thin plate, subjected to tension loading, is analyzed. Numerical results show that the developed numerical tool allows to correctly capture the commonly observed unstable superelastic behavior characterized by nucleation and propagation of martensitic phase. They also show the influence of the internal length parameter, appearing in the nonlocal model, on the size of the localization area and the stress nucleation peak.
The paper is organized as follows. In section 2, the local model is presented and its prediction capability is illustrated through the simulation of an SMA material response, for both martensitic and austenite initial states, under tension and complexe loadings. The obtaining of the nonlocal behavior model is then explained in section 3, before detailing in section 4, the weak formulation of the treated problem, its spatial finite element discretization and the related numerical resolution procedures. In the last section, numerical results and discussion are proposed before ending this paper with concluding remarks.

2. SMA local constitutive model

Constitutive equations describing the thermomechanical behavior of SMA material (NiTi) are summarized in this section. They were obtained by (Peultier et al., 2006) within a local context from an expression of Gibbs free energy

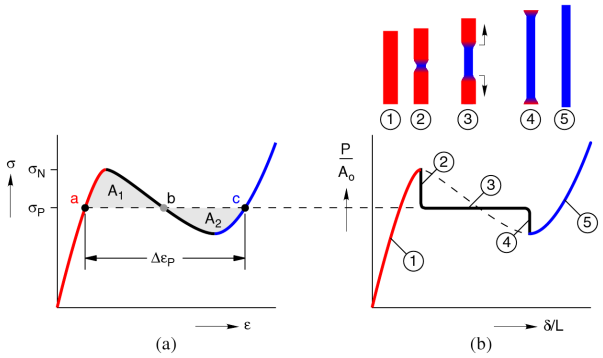

Figure 1: Schematics of transformation localization effect due to (Churchill et al., 2009): (a) local stress-strain (b) global force-elongation and the configuration of the sample before, during and after the phase transformation from austenite to martensite.

potential. Based on micromechanical considerations, this free energy potential takes into account the interactions between and inside grains in an averaged way. It uses two internal variables so as to define the inelastic strain induced by martensitic phase transformation and martensitic variants reorientation. The first internal variable is a scalar quantity, $f = \frac{V_M}{V}$, corresponding to the mean volume fraction of martensite in the REV and defined as the ratio between the volume V_M of martensite and the total volume V of the REV. The second internal variable is a second order tensor, $\overline{\varepsilon}^T = \frac{1}{V_M}\int_{V_M} \varepsilon^T(r)dr$, describing in an averaged way the transformation strain in the REV ($\varepsilon^T(r)$ is the transformation strain at a given material point (r) of the REV). These two internal variables are constrained by two conditions reflecting physical limitations; $0 \leq f \leq 1$ and $\overline{\varepsilon}^T_{eq} = \sqrt{\frac{2}{3}\overline{\varepsilon}^T_{ij}\overline{\varepsilon}^T_{ij}} \leq \overline{\varepsilon}^{Sat}$, where $\overline{\varepsilon}^{Sat}$ is a material parameter characterizing the maximum transformation strain. Based on these internal variables, the following definition,

$$E^T_{ij} = f\overline{\varepsilon}^T_{ij} \tag{1}$$

of the macroscopic transformation strain E^T is adopted. It corresponds to the inelastic strain induced by martensitic transformation, that contributes to the total strain E in the REV according to the additive decomposition:

$$E_{ij} = E^{el}_{ij} + E^{th}_{ij} + E^T_{ij} \tag{2}$$

where E^{el} and E^{th} are respectively the elastic and thermal strains.

In this approach, the phase transformation occurring in the REV is assumed to be completely characterized by the knowledge of the thermodynamic potential, which is here the Gibbs free energy G. The following expression of its variation from the initial state is adopted:

$$\begin{aligned}\Delta G = &- \Delta T S^A + B\left(T - T_0\right) f - \frac{1}{2}\Sigma_{ij} S_{ijkl} \Sigma_{kl} - f\Sigma_{ij}\overline{\varepsilon}^T_{ij} \\ &- \Sigma_{ij}\alpha\delta_{ij}\left(T - T_{ref}\right) + \frac{1}{2} f H_f f^2 + \frac{1}{2} f H_\varepsilon \overline{\varepsilon}^T_{ij}\overline{\varepsilon}^T_{ij}\end{aligned} \tag{3}$$

Where S^A is the entropy of the austenitic phase, $B = -\Delta S$ is the difference between entropies of austenite and martensite, it is also related to the stress-temperature slope of transformation limits, T is the current temperature, T_0 is the equilibrium temperature of martensitic phase transformation, H_f and H_ε are interaction terms taking into account in an averaged way the incompatibilities between respectively martensite variants and grains, Σ is the macroscopic stress tensor, S is the elastic fourth order compliance tensor, α is the thermal expansion coefficient under an isotropic conduction assumption.
The expression of ΔG which was proposed by (Peultier et al., 2006) starting from a micromechanical description of a Martensite-Austenite biphasic REV, accounts for the mechanical, thermal and chemical exchanges. It is a function of control (Σ and T) and internal (f and $\overline{\varepsilon}^T$) macroscopic variables. Driving forces associated to these state variables then arise from the free energy expression (Eq. 3) as follows:

$$F_{\Sigma ij} = -\frac{\partial \Delta G}{\partial \Sigma_{ij}} = S_{ijkl}\Sigma_{kl} + \alpha\delta_{ij}\left(T - T_{ref}\right) + f\overline{\varepsilon}^T_{ij} \tag{4}$$

$$F_f = -\frac{\partial \Delta G}{\partial f} = -B\left(T - T_0\right) + \Sigma_{ij}\overline{\varepsilon}^T_{ij} - \frac{1}{2} H_\varepsilon \overline{\varepsilon}^T_{ij}\overline{\varepsilon}^T_{ij} - H_f f - \lambda_0 - \lambda_1 \tag{5}$$

$$F_{\overline{\varepsilon}^T_{ij}} = -\frac{\partial \Delta G}{\partial \overline{\varepsilon}^T_{ij}} = f\left(\Sigma^{dev}_{ij} - H_\varepsilon \overline{\varepsilon}^T_{ij} - \lambda^\varepsilon_{ij}\right) \tag{6}$$

where Σ^{dev}_{ij} is the deviatoric stress tensor. The coefficients λ_0, λ_1 and λ^ε_{ij} are three Lagrangian multipliers related to the physical limitations of internal variables. They are replaced in the model by the following penalization functions,

$$\lambda_0(f) = \alpha_0 \frac{f-1}{f},\ \lambda_1(f) = \alpha_1 \frac{f}{1-f} \text{ and } \lambda^\varepsilon_{ij} = \text{function of } (\overline{\varepsilon}^T_{ij}, \overline{\varepsilon}^T_{eq}, \overline{\varepsilon}^{Sat}) \tag{7}$$

which are numerically easiest to manage as they allow for a smoother transition between the elastic and phase transformation regimes. The parameters α_0 and α_1 dictate the "degree of smoothness" of this transition.
In agreement with the second principle of thermodynamics, the first driving force (Eq. 4) is set equal to the total macroscopic strain E in order to express the elastic strain accommodation. It leads to the same relation as (Eq. 2) defining the additive decomposition of E. Moreover, the other driving forces (eqs. 5 and 6) shall reach yield values so that the dissipative processes of phase transformation and orientation are activated. The driving force associated to $\overline{\varepsilon}^T_{ij}$ depends only on the deviatoric part of the stress tensor as the phase transformation is

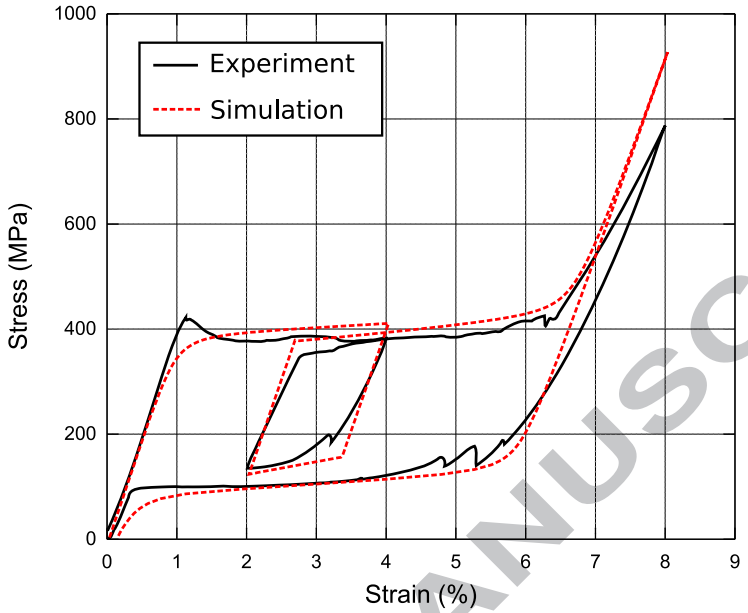

Figure 2: Superelastic behavior under tension loading/unloading.

assumed to occur without volume variation ($\bar{\varepsilon}^T_{kk} = 0$). The hysteresis effect is introduced by considering, during loading and unloading, different values of yield forces, governing the phase transformation or the martensite reorientation. Additional features are introduced in the model in order to describe the internal loop behaviors, (Peultier et al., 2006). Finally, by considering normality and consistency rules, the nonlinear constitutive equations are derived. They are numerically solved by an implicit scheme based on the classical return-mapping and the Newton-Raphson methods.

To illustrate the prediction capability of the present model, it is used to simulate the NiTi SMA material response under proportional and complex thermomechanical cyclic loadings. The model predictions are then compared to experimental measurements which were obtained by (Sittner, 2008) and (Grabe and Bruhns, 2009) for respectively tension and tension-torsion loadings. In Figure 2, the model response is compared to the experience in the case of an initially austenitic material submitted to tension loading/unloading cycle. It shows that the model well describes the whole superelastic behavior (start and finish of transformation, hysteresis size, internal loop size). However it doesn't detect the transformation localization pick and the plateau induced by transformation propagation. The same remarks can be made for the shape memory effect behavior presented in figure 3. It corresponds to the response of an initially martensitic NiTi SMA, submitted to tension loading/unloading. Figure 4 displays the model predictions in the case of a butterfly non proportional loading

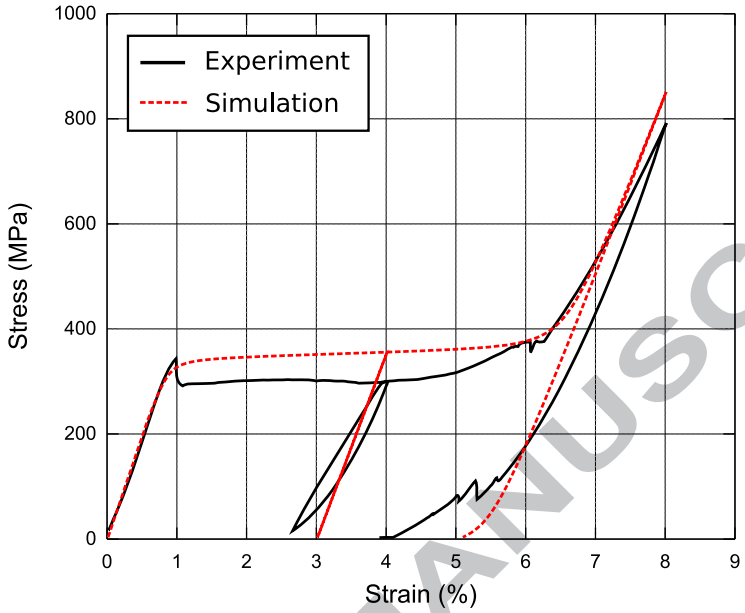

Figure 3: Shape memory effect behavior under tension loading/unloading.

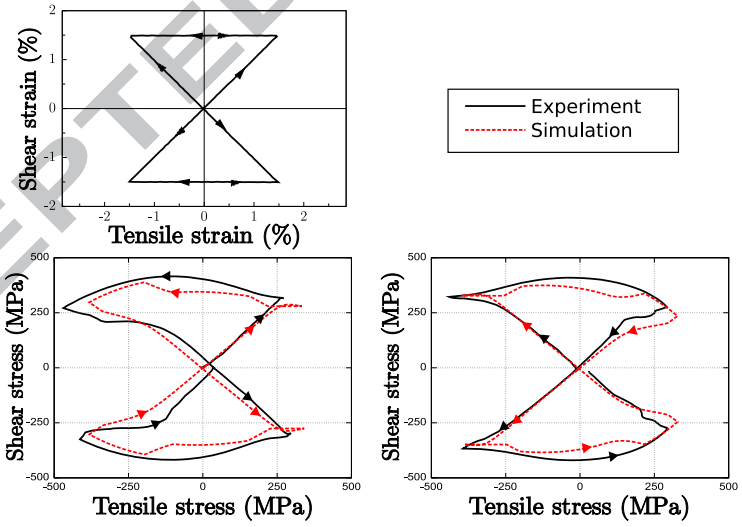

Figure 4: Comparison between the local model predictions and the experiments in the case of complex loading for two different directions of the deformation.

for two different directions of the deformation. It shows that the model correctly describes the thermomechanical behavior under such complex loading.
In the following, the presented local model is considered as a base for a nonlocal formulation in the case of pseudoelastic behavior. For that reason the part related to memory effect behavior in the potential function (Eq. 3) is ignored.

3. SMA nonlocal constitutive model

As stated in the introduction, a constitutive local approach such as the one detailed above, will lead to a mesh sensitive material response if the resulting model is used to describe a material behavior with softening. From the mathematical point of view, this pathological effect is explained by the loss of ellipticity of the governing local equations (no well-posedness condition) in presence of softening. This also can be interpreted as the absence in the model governing equations of any reference to an internal length, meaning that the material heterogeneity is insufficiently well described. A possible way to overcome this difficulty at the continuum level is to use nonlocal definition of the material point response, so as to account for the material inhomogeneity. The point local response then depends on the interactions of this point with its neighborhood, besides on its specific loading history. Practically, a localization limiter is brought by the nonlocal formulation, that prevents the singular character of the constitutive response in presence of softening.
Classically, there exist two kinds of nonlocal strategies: the integral and gradient formulations. The integral formulations are known to ensure a strong type of nonlocality, i.e. long range interactions between the material point and its neighborhood, while in gradient formulations, only short range interactions are represented. The emergence of these different approaches and their applications in elasticity, plasticity or damage, are detailed by (Jirásek and Bažant, 2002).
Recently, an implicit gradient modelling method, that preserves a strong nonlocality, has been proposed by (Peerlings et al., 2001) for damage, before being used by (Engelen et al., 2003) for nonlocal continuum plasticity. The benefits of such approach is a priori its capability to consider the possible interactions of a material point with all the remaining domain. That might be relevant in our sense for capturing size effects. In this work, similar nonlocal approach is adopted in order to establish a gradient model of SMA behavior. Only the pseudoelasticity case is treated.

3.1. Constitutive equations for an unstable superelastic behavior

The local superelastic behavior is described by a simplified expression of the Gibbs free energy proposed by (Peultier et al., 2006), where the effect of reorientation and expansion are ignored. Only the phase transformation inducing an oriented martensite under a mechanical loading is considered. In this case, the martensite variants are oriented by the deviatoric part of the applied stress Σ_{ij}^D. The macroscopic transformation strain defined in (Eq. 1) becomes:

$$E_{ij}^{T} = \frac{3}{2}\frac{\Sigma_{ij}^{D}}{\Sigma_{eq}} f \overline{\varepsilon}_{sat}^{T} \tag{8}$$

where Σ_{eq} is the Von Mises equivalent macroscopic stress, and $\overline{\varepsilon}_{sat}^{T}$ is the saturation value of the mean transformation strain.

Substituting (Eq. 8) in (Eq. 3) and considering only the isothermal case, lead to the following expression of ΔG:

$$\Delta G = B\left(T - T_0\right) f - \frac{1}{2}\Sigma_{ij} S_{ijkl} \Sigma_{kl} - \Sigma_{eq} f \overline{\varepsilon}_{sat}^{T} + \frac{1}{2} H_f f^2 \tag{9}$$

The driving force (Eq. 5) associated to the phase transformation process reduces in this case to:

$$F_f = -B\left(T - T_0\right) + \Sigma_{eq}\overline{\varepsilon}_{sat}^{T} - H_f f - \alpha_0 \frac{f-1}{f} - \alpha_1 \frac{f}{1-f} \tag{10}$$

The transformation force (Eq. 10) is assumed to satisfy the following dry friction condition :

$$|F_f| \leq F_f^{crit} \tag{11}$$

The phase transformation is activated when $|F_f| = F_f^{crit}$.

3.2. Definition of nonlocal internal variable

In this subsection, the gradient-type definition of the nonlocal internal variable, $\overline{f}$, is derived starting from the classical integral formulation, (Jirásek and Bažant, 2002):

$$\overline{f}\left(\overrightarrow{x}\right) = \int_{\Omega} G\left(\overrightarrow{y}, \overrightarrow{x}\right) f\left(\overrightarrow{y}\right) \mathrm{d}\Omega\left(\overrightarrow{y}\right) \tag{12}$$

In this relation, f is the local field, Ω, the material domain, and $G\left(\overrightarrow{y}, \overrightarrow{x}\right)$, a given nonlocal weight function. Usual expressions of this latter are the Gauss distribution, the bell-shaped functions or the Green's function,

$$G\left(\overrightarrow{y}, \overrightarrow{x}\right) = \frac{1}{4\pi\rho\ell^2} \exp\left(-\frac{\rho}{\ell}\right) \tag{13}$$

which was retained by (Peerlings et al., 2001; Engelen et al., 2003) in their developments owing to its convenient properties. This statement will be detailed a little further.

In the expression (Eq. 13), $\rho = |\overrightarrow{x} - \overrightarrow{y}|$ is the distance between two points, $\overrightarrow{y}$, the position vector of the infinitesimally small volume $\mathrm{d}\Omega$, and ℓ, an internal length parameter of the material, (Fig. 5). The parameter ℓ determines the size of the material volume which effectively contributes to the nonlocal quantity. It is related a priori to the scale of the microstructure and also to geometrical factors, (He and Sun, 2009a,b, 2010).

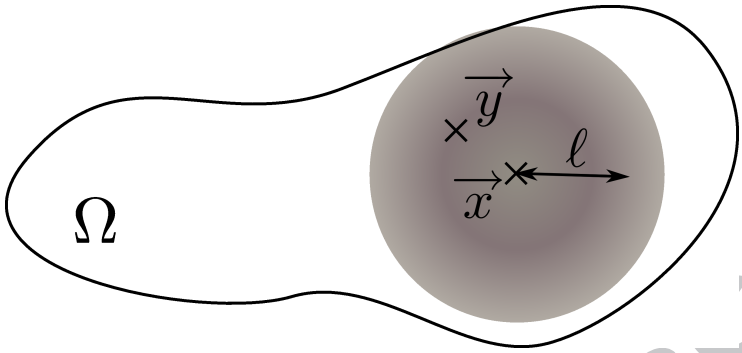

Figure 5: Nonlocal description at a material point.

According to (Pijaudier-Cabot and Bažant, 1987; Peerlings et al., 2001; Engelen et al., 2003), the integral definition above can be approximated by a differential relation based on a Taylor expansion of $f(\overrightarrow{y})$ around the point $\overrightarrow{x}$:

$$\begin{aligned} f(\overrightarrow{y}) =& f(\overrightarrow{x}) + \frac{\partial f}{\partial x_i}(y_i - x_i) + \frac{1}{2!}\frac{\partial^2 f}{\partial x_i \partial x_j}(y_i - x_i)(y_j - x_j) \\ &+ \frac{1}{3!}\frac{\partial^3 f}{\partial x_i \partial x_j \partial x_k}(y_i - x_i)(y_j - x_j)(y_k - x_k) \\ &+ \frac{1}{4!}\frac{\partial^4 f}{\partial x_i \partial x_j \partial x_k \partial x_l}(y_i - x_i)(y_j - x_j)(y_k - x_k)(y_l - x_l) \\ &+ \dots \end{aligned} \tag{14}$$

where Einstein's summation convention applies for the indices i, j, k and l. Substituting of this expansion into equation (Eq. 12) and appropriate integrations yield (on $\Omega = R^2$ or $\Omega = R^3$):

$$\overline{f}(\overrightarrow{x}) = f(\overrightarrow{x}) + c(\ell)\nabla^2 f(\overrightarrow{x}) + d(\ell)\nabla^4 f(\overrightarrow{x}) + \dots \tag{15}$$

where $\nabla^2 = \sum_i \frac{\partial^2}{\partial x_i^2}$ is the laplacian operator, $c(\ell) = \frac{1}{2}\int_\Omega G(\overrightarrow{y}, \overrightarrow{x})(y_i - x_i)^2 \, \mathrm{d}\Omega(\overrightarrow{y})$, and $d(\ell) = \frac{1}{4!}\int_\Omega G(\overrightarrow{y}, \overrightarrow{x})(y_i - x_i)^4 \, \mathrm{d}\Omega(\overrightarrow{y})$. It was shown by (Peerlings et al., 2001; Engelen et al., 2003) that $c(\ell) = \ell^2$ and $d(\ell) = \ell^4$.

Relation (Eq. 15) represents a gradient-based definition of the nonlocal variable $\overline{f}$. The gradient parameters c and d appearing in this relation come from integrations of the Green's function G (Eq. 13), weighted by Taylor's expansion terms at different orders. Note that these parameters have the dimension of length to an even power and that the odd derivatives vanish due to the isotropy of G.

Equation (Eq. 15) stands for an explicit definition of $\overline{f}$ as this latter is directly computed from the local quantity f and its gradients. According to (Peerlings et al., 2001), this explicit gradient formulation belongs to the class

of weakly nonlocal theory in the sense that the constitutive response of each material point depends only on an infinitesimal neighborhood of that point (as the gradient can be calculated from the distribution of the function in an arbitrarily small neighborhood). Strong nonlocality can theoretically be recovered if sufficient higher order terms of the Taylor development are taken into account in the definition of $\overline{f}$. This procedure will require the use of nonstandard finite elements of high regularity and will prove very much time consuming. To avoid these numerical inconveniences, (Peerlings et al., 2001) and (Engelen et al., 2003) proposed another way of nonlocality enhancement applied for respectively damage and plasticity. This approach named as implicit gradient method will be adopted hereafter for SMAs. First, the laplacian of equation (Eq. 15) is considered:

$$\nabla^2 \overline{f}\left(\overrightarrow{x}\right) = \nabla^2 f\left(\overrightarrow{x}\right) + c\left(\ell\right) \nabla^4 f\left(\overrightarrow{x}\right) + \dots \tag{16}$$

Multiplying the equation (Eq. 16) by $c\left(\ell\right)$,

$$c\left(\ell\right) \nabla^2 \overline{f}\left(\overrightarrow{x}\right) = c\left(\ell\right) \nabla^2 f\left(\overrightarrow{x}\right) + c^2\left(\ell\right) \nabla^4 f\left(\overrightarrow{x}\right) + \dots \tag{17}$$

and subtracting the result (Eq. 17) from (Eq. 15) leads to:

$$\overline{f}\left(\overrightarrow{x}\right) - c\left(\ell\right) \nabla^2 \overline{f}\left(\overrightarrow{x}\right) = f\left(\overrightarrow{x}\right) + \left(d\left(\ell\right) - c^2\left(\ell\right)\right) \nabla^4 f\left(\overrightarrow{x}\right) + \dots \tag{18}$$

As it was shown by (Peerlings et al., 2001; Engelen et al., 2003), the results $c\left(\ell\right) = \ell^2$ and $d\left(\ell\right) - c^2\left(\ell\right) = 0$ hold for any field $f\left(\overrightarrow{x}\right)$ when using the Green's weight function (Eq. 13). Moreover, higher order terms of equation (Eq. 18) can be neglected in this case according to the same authors. The implicit definition of $\overline{f}$ now reads:

$$\overline{f}\left(\overrightarrow{x}\right) - c\left(\ell\right) \nabla^2 \overline{f}\left(\overrightarrow{x}\right) = f\left(\overrightarrow{x}\right) \tag{19}$$

which reduces to the local field if $\ell \to 0$ ($\overline{f} = f$).

It is noteworthy to see that the weight function (Eq. 13) used by (Peerlings et al., 2001; Engelen et al., 2003) was not arbitrarily chosen as this function corresponds to the Green's function of the PDE (Eq. 19), determined by (Zauderer, 1989), to which the nonlocal quantity $\overline{f}$ obeys. This function allows the obtaining of a close differential approximation of the integral (Eq. 12), that respects the properties of this latter. This a posteriori justifies the choice of (Eq. 13) as a weight function.

The partial derivative equation (Eq. 19) defining the nonlocal phase transformation is completed by appropriate boundary conditions concerning $\overline{f}$ or its gradient. We consider the following Neumann type boundary condition at the material domain border Γ, Fig. 6:

$$\overrightarrow{\nabla} \overline{f} = \overrightarrow{0} \quad \text{on} \quad \Gamma \tag{20}$$

This homogeneous boundary condition stats that no evolution of the transformation front is admitted at the domain border, and leads in combination with the equation (Eq. 19) to,

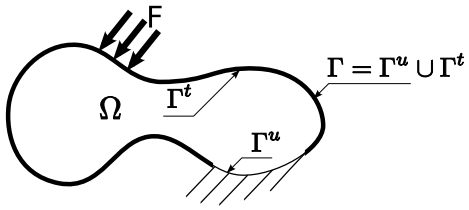

Figure 6: Considered domain Ω and its boundary Γ.

$$\int_\Omega \overline{f} \mathrm{d}\Omega = \int_\Omega f \mathrm{d}\Omega \tag{21}$$

which means that the total quantity of martensite is the same for local and nonlocal formulations.

The nonlocal definition (Eq. 19) of the model internal variable $\overline{f}$ provides a localization limiter in presence of unstable softening behavior, such as the one highlighted by (Shaw and Kyriakides, 1995) and schematically illustrated in Fig. 1. To include the softening description in the present approach, the critical transformation force parameter, that corresponds to the value of the driving force (Eq. 6) which activates the transformation, is modified as follows:

$$F_f^{crit} = F_{f\,0}^{crit} \exp\left(-H_{\overline{f}} \overline{f}\right) \tag{22}$$

It assumes that the yield force of transformation decreases from its initial value along with the transformation progression. $H_{\overline{f}}$ is a material parameter that controls the decreasing of the critical force.

In summary the nonlocal constitutive equations of the superelasticity SMA behavior are listed in Table 1.

4. Variational form of the governing equations

The variational (weak) form of the governing equations (Table 1) is achieved as a preliminary step to finite element implementation. For this purpose, two functional spaces of appropriate test (virtual) functions are defined:

$$\begin{aligned} W_u &= \left\{ \overrightarrow{w}_u / \overrightarrow{w}_u \in \left[C^0\right]^{p\,1}, \overrightarrow{w}_u = \overrightarrow{0} \text{ where the displacement } u \text{ is prescribed} \right\} \\ W_{\overline{f}} &= \left\{ w_{\overline{f}} / w_{\overline{f}} \in \left[C^0\right], w_{\overline{f}} = 0 \text{ where the martensite fraction } \overline{f} \text{ is prescribed} \right\} \end{aligned} \tag{23}$$

[1] p is the problem dimension

Pre-multiplying the field equations (Table 1) by the test functions and integrations over the domain Ω yield:

$$\int_\Omega \overrightarrow{w}_u \cdot \left(\overrightarrow{\nabla} \cdot \mathbf{\Sigma}\right) \mathrm{d}\Omega = 0 \qquad \forall \overrightarrow{w}_u \in W_u \tag{24}$$

and

$$\int_\Omega w_{\overline{f}} \left(\overline{f} - \ell^2 \nabla^2 \overline{f}\right) \mathrm{d}\Omega = \int_\Omega w_{\overline{f}} f \mathrm{d}\Omega \qquad \forall w_{\overline{f}} \in W_{\overline{f}} \tag{25}$$

Applying the divergence theorem and taking into account the boundary conditions and the symmetry of the stress tensor give:

$$\int_\Omega \left[\overrightarrow{\nabla} \overrightarrow{w}_u\right]^T : \mathbf{\Sigma} \mathrm{d}\Omega = \int_{\Gamma^t} \overrightarrow{w}_u \cdot \overrightarrow{T}^u \mathrm{d}\Gamma \qquad \forall \overrightarrow{w}_u \in W_u \tag{26}$$

$$\int_\Omega \left(w_{\overline{f}} \overline{f} + \ell^2 \overrightarrow{\nabla} w_{\overline{f}} \cdot \overrightarrow{\nabla} \overline{f}\right) \mathrm{d}\Omega = \int_\Omega w_{\overline{f}} f \mathrm{d}\Omega \qquad \forall w_{\overline{f}} \in W_{\overline{f}} \tag{27}$$

These equations are solved numerically in their incremental forms,

$$\begin{aligned} &\int_\Omega \left[\overrightarrow{\nabla} \overrightarrow{w}_u\right]^T : \left(H^{uu} : \delta E\right) \mathrm{d}\Omega + \int_\Omega \left[\overrightarrow{\nabla} \overrightarrow{w}_u\right]^T : \left(H^{u\overline{f}} \delta \overline{f}\right) \mathrm{d}\Omega \\ &= \int_{\Gamma^u} \overrightarrow{w}_u \cdot \overrightarrow{T}^{u\,(i)} \mathrm{d}\Gamma - \int_\Omega \left[\overrightarrow{\nabla} \overrightarrow{w}_u\right]^T : \mathbf{\Sigma}^{(i-1)} \mathrm{d}\Omega \end{aligned} \tag{28}$$

$$\begin{aligned} &- \int_\Omega w_{\overline{f}} H^{\overline{f}u} : \delta E \mathrm{d}\Omega + \int_\Omega \left[w_{\overline{f}} \left(1 - H^{\overline{f}\overline{f}}\right) \delta \overline{f} + \ell^2 \overrightarrow{\nabla} w_{\overline{f}} \cdot \overrightarrow{\nabla} \delta \overline{f}\right] \mathrm{d}\Omega \\ &= - \int_\Omega \left[w_{\overline{f}} \overline{f}^{(i-1)} + \ell^2 \overrightarrow{\nabla} w_{\overline{f}} \cdot \overrightarrow{\nabla} \overline{f}^{(i-1)}\right] \mathrm{d}\Omega + \int_\Omega w_{\overline{f}} f^{(i-1)} \mathrm{d}\Omega \end{aligned} \tag{29}$$

which are obtained by using the following linearizations of $\mathbf{\Sigma}$ and f:

$$\mathbf{\Sigma}^{(i)} = \mathbf{\Sigma}^{(i-1)} + \delta \mathbf{\Sigma}, \quad f^{(i)} = f^{(i-1)} + \delta f \tag{30}$$

where the increments $\delta \mathbf{\Sigma}$ and δf read:

$$\left\{ \begin{array}{rcl} \delta \Sigma_{ij} & = & H^{uu}_{ijkl} \delta E_{kl} + H^{u\overline{f}}_{ij} \delta \overline{f} \\ \delta f & = & H^{\overline{f}u}_{kl} \delta E_{kl} + H^{\overline{f}\overline{f}} \delta \overline{f} \end{array} \right. \tag{31}$$

They are derived in a consistent way from the driving forces (Table 1) thanks to the tangent operators :

$$\begin{aligned} H^{uu}_{ijkl} &= \frac{\partial \Sigma_{ij}}{\partial E_{kl}} \qquad H^{u\overline{f}}_{ij} = \frac{\partial \Sigma_{ij}}{\partial \overline{f}} \\ H^{\overline{f}u}_{kl} &= \frac{\partial f}{\partial E_{kl}} \qquad H^{\overline{f}\overline{f}} = \frac{\partial f}{\partial \overline{f}} \end{aligned} \tag{32}$$

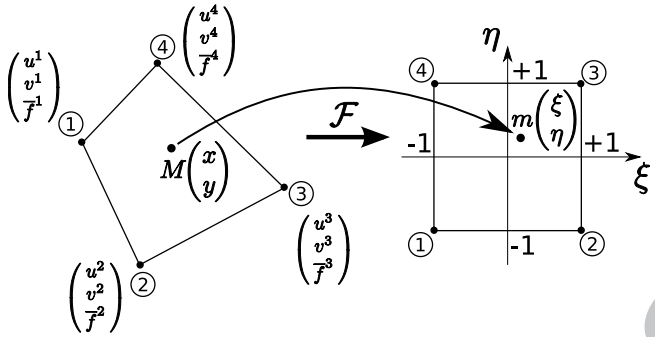

Figure 7: Transition from a structural quadrangular finite element to a reference element by transformation $\mathcal{F}$.

The integral equations (Eqs. 28 and 29) will be solved numerically by using the finite element method within the `Abaqus`® software in 1D and 2D cases. For that purpose, two specific finite elements are developed and implemented in `Abaqus`® through the user's subroutine UEL. Thereafter, the finite element discretization of the equations for 2D problems under plane stress conditions is detailed.

4.1. Finite element spatial discretization for 2D problems

In this case, a solid isoparametric quadrangular finite element with 4 nodes is developed. It uses the following bilinear shape functions,

$$\begin{aligned} N_1(\xi,\eta) &= \frac{(1-\xi)(1-\eta)}{4} \\ N_2(\xi,\eta) &= \frac{(1+\xi)(1-\eta)}{4} \\ N_3(\xi,\eta) &= \frac{(1+\xi)(1+\eta)}{4} \\ N_4(\xi,\eta) &= \frac{(1-\xi)(1+\eta)}{4} \end{aligned} \tag{33}$$

in order to interpolate the displacement and the nonlocal martensite volume fraction (unknown fields) inside the element as:

$$\overrightarrow{u}(\xi,\eta) = [N_N^u]\{u^N\} \tag{34}$$

$$\overline{f}(\xi,\eta) = \left[N_N^{\overline{f}}\right]\left\{\overline{f}^N\right\} \tag{35}$$

In (Eq. 34) and (Eq. 35), (ξ,η) is a given point inside the reference element, Fig. 7, $\left(\{u^N\}, \left\{\overline{f}^N\right\}\right)$ and $\left([N_N^u], \left[N_N^{\overline{f}}\right]\right)$ are respectively nodal vectors and interpolation matrices defined as:

$$\left\{u^N\right\} = \left\{\begin{array}{c} u^1 \\ v^1 \\ u^2 \\ v^2 \\ u^3 \\ v^3 \\ u^4 \\ v^4 \end{array}\right\} \quad \text{and} \quad \left\{\overline{f}^N\right\} = \left\{\begin{array}{c} \overline{f}^1 \\ \overline{f}^2 \\ \overline{f}^3 \\ \overline{f}^4 \end{array}\right\} \tag{36}$$

and

$$\begin{aligned} \left[N_N^u(\xi,\eta)\right] &= \left[\begin{array}{cccccccc} N_1 & 0 & N_2 & 0 & N_3 & 0 & N_4 & 0 \\ 0 & N_1 & 0 & N_2 & 0 & N_3 & 0 & N_4 \end{array}\right] \\ \left[N_N^{\overline{f}}(\xi,\eta)\right] &= \left[\begin{array}{cccc} N_1 & N_2 & N_3 & N_4 \end{array}\right] \end{aligned} \tag{37}$$

The strain tensor E_{ij} and the gradient vector of the nonlocal martensite volume fraction $\overrightarrow{\nabla}\overline{f}$ are also interpolated inside the element, which leads to the following expressions of these quantities:

$$\{E\} = \left\{\begin{array}{c} E_{xx} \\ E_{yy} \\ 2E_{xy} \end{array}\right\} = \left[B_N^u\right]\left\{u^N\right\} \quad \text{and} \quad \left\{\overrightarrow{\nabla}\overline{f}\right\} = \left\{\begin{array}{c} \overline{f}_{,x} \\ \overline{f}_{,y} \end{array}\right\} = \left[B_N^{\overline{f}}\right]\left\{\overline{f}^N\right\} \tag{38}$$

Expressions of matrices $\left[B_N^u\right]$ and $\left[B_N^{\overline{f}}\right]$ are given in appendix.

Introducing the interpolation matrices of strain and gradient of martensite nonlocal fraction in weak equations of equilibrium (Eq. 28) and (Eq. 29) gives:

$$\begin{aligned} &\int_\Omega \left[B_N^u\right]^T \left[H^{uu}\right]\left[B_N^u\right] \mathrm{d}\Omega \left\{\delta u^N\right\} + \int_\Omega \left[B_N^u\right]^T \left[H^{u\overline{f}}\right]\left[N_N^{\overline{f}}\right] \mathrm{d}\Omega \left\{\delta\overline{f}^N\right\} \\ &= -\int_\Omega \left[B_N^u\right]^T \left\{\Sigma^{(i-1)}\right\} \mathrm{d}\Omega + \int_\Gamma \left[N_N^u\right]^T \left\{T^{(i)}\right\} \mathrm{d}\Gamma \end{aligned} \tag{39}$$

$$\begin{aligned} &-\int_\Omega \left[N_N^{\overline{f}}\right]^T \left[H^{\overline{f}u}\right]\left[B_N^u\right] \mathrm{d}\Omega \left\{\delta u^N\right\} - \int_\Omega \left[N^{\overline{f}_N}\right] H^{\overline{f}\overline{f}} \left[N_N^{\overline{f}}\right] \mathrm{d}\Omega \left\{\delta\overline{f}^N\right\} \\ &+ \int_\Omega \left[N_N^{\overline{f}}\right]^T \left[N_N^{\overline{f}}\right] \mathrm{d}\Omega \left\{\delta\overline{f}^N\right\} + \int_\Omega \ell^2 \left[B_N^{\overline{f}}\right]^T \left[B_N^{\overline{f}}\right] \mathrm{d}\Omega \left\{\overline{f}^N\right\} \\ &= \int_\Omega \left[N_N^{\overline{f}}\right]^T f^{(i-1)} \mathrm{d}\Omega - \int_\Omega \left[N_N^{\overline{f}}\right]^T \left[N^{\overline{f}}\right] \left\{\overline{f}^{N\,(i-1)}\right\} \mathrm{d}\Omega \\ &- \int_\Omega \ell^2 \left[B_N^{\overline{f}}\right]^T \left[B_N^{\overline{f}}\right] \left\{\overline{f}^{N\,(i-1)}\right\} \mathrm{d}\Omega \end{aligned} \tag{40}$$

which can be expressed as follows,

$$\left\{\begin{array}{lcl} \left[K^{uu}\right]\left\{\delta u^N\right\}+\left[K^{u\overline{f}}\right]\left\{\delta\overline{f}^N\right\} &=& -\left\{F^u_{int}\right\}+\left\{F^u_{ext}\right\} \\ \left[K^{\overline{f}u}\right]\left\{\delta u^N\right\}+\left[K^{\overline{f}\overline{f}}\right]\left\{\delta\overline{f}^N\right\} &=& -\left\{F^{\overline{f}}_{int}\right\} \end{array}\right. \tag{41}$$

by introducing the following tangent submatrices, nodal internal forces, and nodal external forces:

$$\begin{aligned} \left[K^{uu}\right] &= \int_\Omega \left[B^u_N\right]^T\left[H^{uu}\right]\left[B^u_N\right]\mathrm{d}\Omega \\ \left[K^{u\overline{f}}\right] &= \int_\Omega \left[B^u_N\right]^T\left[H^{u\overline{f}}\right]\left[N^{\overline{f}}_N\right]\mathrm{d}\Omega \\ \left[K^{\overline{f}u}\right] &= -\int_\Omega \left[N^{\overline{f}}_N\right]^T\left[H^{\overline{f}u}\right]\left[B^u_N\right]\mathrm{d}\Omega \\ \left[K^{\overline{f}\overline{f}}\right] &= -\int_\Omega \left[N^{\overline{f}}_N\right]^T H^{\overline{f}\overline{f}}\left[N^{\overline{f}}_N\right]\mathrm{d}\Omega+\int_\Omega\left[N^{\overline{f}}_N\right]^T\left[N^{\overline{f}}_N\right]\mathrm{d}\Omega \\ &\quad +\int_\Omega \ell^2\left[B^{\overline{f}}_N\right]^T\left[B^{\overline{f}}_N\right]\mathrm{d}\Omega \\ \left\{F^u_{int}\right\} &= \int_\Omega \left[B^u_N\right]^T\left\{\Sigma^{(i-1)}\right\}\mathrm{d}\Omega \\ \left\{F^u_{ext}\right\} &= \int_\Gamma \left[N^u_N\right]^T\left\{T^{(i)}\right\}\mathrm{d}\Gamma \\ \left\{F^{\overline{f}}_{int}\right\} &= -\int_\Omega\left[N^{\overline{f}}_N\right]^T f^{(i-1)}\mathrm{d}\Omega+\int_\Omega\left[N^{\overline{f}}_N\right]^T\left[N^{\overline{f}}_N\right]\left\{\overline{f}^{N\,(i-1)}\right\}\mathrm{d}\Omega \\ &\quad +\int_\Omega \ell^2\left[B^{\overline{f}}_N\right]^T\left[B^{\overline{f}}_N\right]\left\{\overline{f}^{N\,(i-1)}\right\}\mathrm{d}\Omega \end{aligned} \tag{42}$$

It should be noticed that in (Eq. 41), no external force is applied for the sub-system governing the nonlocal martensite volume fraction variation since the corresponding natural-type boundary condition is implicitly verified in the weak balance formulation.

The stiffness submatrices $\left[K^{ij}\right]$ as well as the nodal internal forces and the nodal external forces are evaluated numerically by using the classical Gauss full integration method. They are expressed as sums of their values at Gauss points weighted by ω_i given in Table 2. For example, $[K^{uu}]$ reads:

$$\left[K^{uu}\right]=\sum_{i=1}^{4}\omega_i\left[B^u_N\left(\xi_i,\eta_i\right)\right]^T\left[H^{uu}\left(\xi_i,\eta_i\right)\right]\left[B^u_N\left(\xi_i,\eta_i\right)\right]\det\left(\left[\mathcal{J}\left(\xi_i,\eta_j\right)\right]\right) \tag{43}$$

where $\mathcal{J}$ is a jacobian matrix which is detailed in appendix.

Based on this formulation, a quadrilateral plane stress finite element is developed and implemented in `Abaqus`®. Similar approach is also used to develop an 1D finite element. The implementation of these elements in `Abaqus`® is described in the following section with an insight on the numerical procedure of resolution.

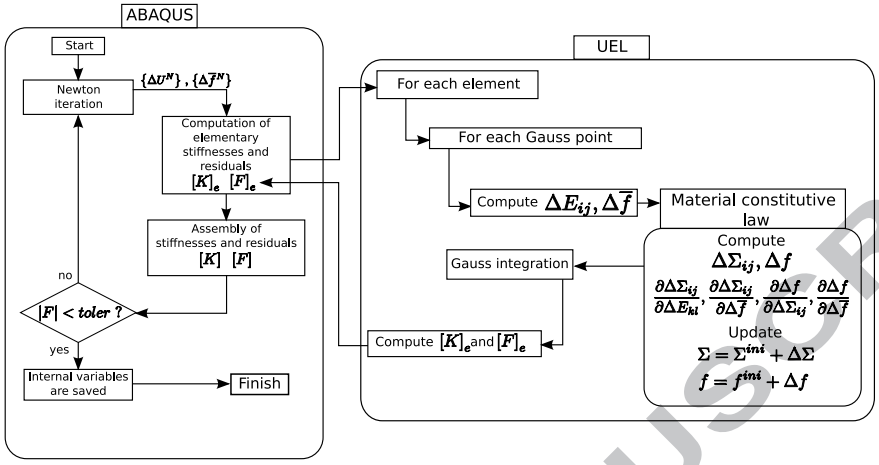

Figure 8: Schematic of the resolution procedure in Abaqus®.

4.2. Solution procedure and implementation in Abaqus® of the constitutive equations

The developed finite elements are implemented into the commercial finite element software Abaqus®, through the user subroutine UEL (User ELement). The finite element equations (Eq. 42) are programmed by using the object oriented language C++, which allows the definition of specific numerical objects such as matrices or vectors with a dynamic size. The Simula+ library developed by (Collard et al., 2010) is also used in order to ensure robust algorithm and data structures for tensors and matrices.

The UEL subroutine is called at each element of the structure mesh. Trial values of the nodal degrees of freedom and their increments are given as input data of the user subroutine. User programming returns the nodal residuals sub-vector and tangent sub-matrix of the element. Abaqus® is then in charge to assemble all elementary residuals and matrices to solve the problem on the whole structure. A schematic of the resolution procedure is given in Fig. 8.

From nodal degrees of freedom increments Δu^N and $\Delta \overline{f}^N$, values of strain increment and nonlocal martensite volume fraction increment are computed at each Gauss point using the interpolation matrices. A subprogram similar to a UMAT subroutine in Abaqus® allows us to compute the material response using a Newton-Raphson iterative scheme. The updated values of the stress tensor $\boldsymbol{\Sigma}$, the local martensite volume fraction f, and the tangent operators $\frac{\partial \Delta \boldsymbol{\Sigma}}{\partial \Delta \mathbf{E}}$, $\frac{\partial \Delta \boldsymbol{\Sigma}}{\partial \Delta \overline{f}}$, $\frac{\partial \Delta f}{\partial \Delta \mathbf{E}}$ and $\frac{\partial \Delta f}{\partial \Delta \overline{f}}$ are used in the computation of the elementary stiffness matrices and residual vectors.

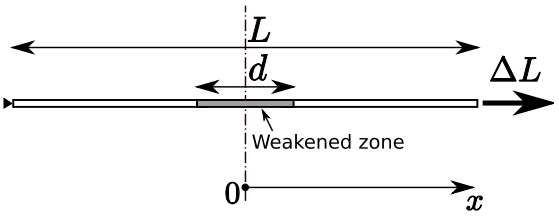

L	200 mm
d	40 mm
S	1.3 mm^2
B	5 MPa/°C
T	25 °C
T_0	-40 °C
$F_{f_0}^{crit}$	150 MPa (nom.)
$F_{f_0}^{crit}$	140 MPa (weak)
H_f	1 MPa
$H_{\overline{f}}$	4
Y	70 000 MPa
ε_{SAT}^{T}	0.05
α_0	0.1 MPa
α_1	0.1 MPa

Figure 9: Tensile test of an SMA wire with imperfection and material parameters.

5. Results and discussion

1D and 2D simulations are carried out in order to demonstrate the ability of the developed gradient model to cope with softening behavior in SMA wire and thin plate during stress-induced martensite transformation. The model parameters are identified by using experimental data from (Sittner, 2008).

5.1. Tensile test on SMA wire

The response of an SMA wire, submitted to tension loading so as to attain 6 % of total averaged strain, is predicted by using the developed 1D finite element within `Abaqus`®. The geometric properties and the model parameters are given in Fig. 9.

First, the response of the SMA wire is determined by solving the homogeneous problem without localization, i.e. by considering the structure free from imperfection ($d = 0$ m). The interest of this simulation is to show the role of the function (Eq. 22) that has been adopted to describe the evolution of the critical force during the transformation process. Figure 10 displays the resulting force-displacement curves for different values of the coefficient $H_{\overline{f}}$. We observe that this parameter controls as expected the softening rate.

Next, the width of the imperfection d is given a finite value. Having a reduced value of the yield transformation force, this imperfection will trigger a solution with localization of the deformation (martensitic transformation) at the center of the wire. In this situation, the gradient-enhanced model, unlike local formulation, produces a mesh-independent numerical solution, as can be concluded from the Fig. 11 which shows the force-displacement response and the martensite nonlocal spatial distribution for different mesh densities and $\ell =$ 4 mm. We observe in particular the oscillations on the force-displacement for coarse meshing, and a numerical response which becomes insensitive to meshing

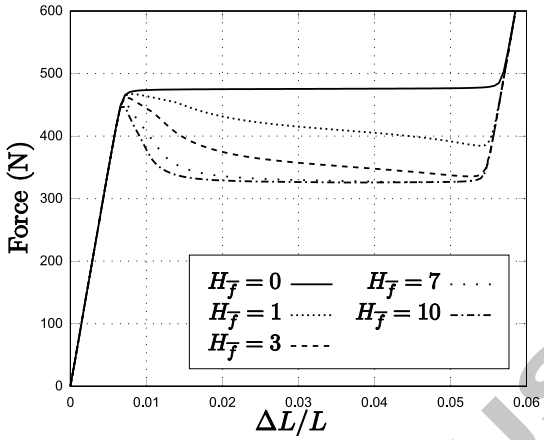

Figure 10: Force-displacement curves for different values of the model parameter $H_{\overline{f}}$.

densities once convergence is reached (for sufficiently refined meshing). These results demonstrate the regularizing effect of the gradient term. The numerical oscillations are observed on the force-displacement response when the internal length parameter ℓ is lower than the element length. To explain these numerical instabilities, we point out the fact that in such case, the localization zone is contained in a single truss element. As the element shape functions are linear, it becomes impossible to describe fairly the variation of the martensite fraction governed in this zone by a second order differential term. The contribution of this term is precisely ignored which leads to a coarse approximation of $\overline{f}$ and consequently of Σ. This feature could be improved by increasing the degree of interpolation or adopting a more refined mesh.

In figures 12 and 13 are respectively depicted, for a given mesh density and different values of ℓ, the force-displacement and the spatial distribution of the nonlocal martensite volume fraction. It can be seen from Fig. 12 the kind of response exhibited by SMA wire undergoing stress-induced martensite transformation, consisting of a stress drop at the beginning of phase transformation followed by a transformation plateau at constant stress, for lower values of the internal length parameter ℓ. The stress peak also becomes steeper when ℓ decreases. This is directly related to the fact that ℓ is a localization limiter. When it tends towards zero, the localization accompanying the softening is restricted to a small part of the structure, and the remaining part unloads elastically as its strength is not altered. In the same figure, the response of the local model ($\ell = 0$)is reported for a purpose of comparison. It was obtained by considering a homogeneous SMA wire (without imperfection, and thus without localization) under direct displacement control.

The influence of the internal length parameter ℓ is also observed in Fig. 13 displaying the spatial distribution of the nonlocal martensite volume fraction. For

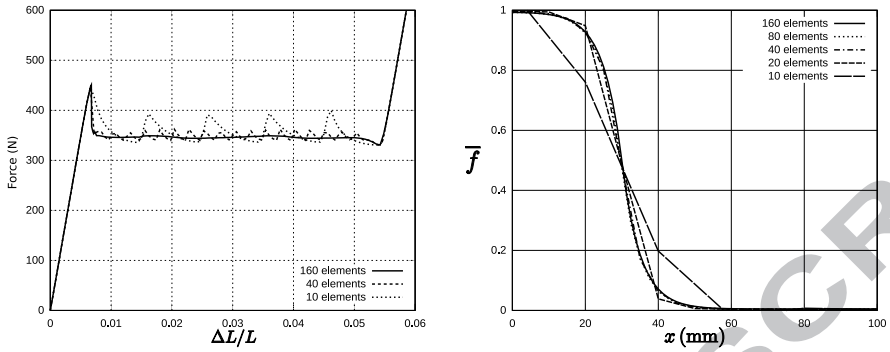

Figure 11: Meshing size influence. (a): on the force-displacement response, (b): on the spatial distribution of nonlocal martensite volume fraction.

lower values of ℓ, the figure 13 shows localization of martensite transformation until saturation in the weakened zone followed by a transformation propagation along the wire. For higher values of ℓ, the localization is attenuated until the spatial distribution of nonlocal volume fraction becomes uniform (no localization) for the highest values of ℓ.

In Fig. 14, the SMA wire response under tension loading/unloading is displayed for different values of ℓ. Note that for the reverse martensite-austenite transformation, the yield force is $F_f^{crit} = F_{f\,0}^{crit} \exp\left(-H_{\overline{f}}(1-\overline{f})\right)$. For a complete unloading, we observe a return to the initial state without any residual stress or strain, a response which is consistent with the superelasticity framework of the study. We observe also from Fig. 14, that the largest is the internal length parameter ℓ, the highest is the dissipated hysteresis energy. In (Sun and He, 2008), it has been reported that the dissipated energy in NiTi SMA increases for larger nanograins. This may suggest that the parameter ℓ can be linked to the grain size.

5.2. Tensile test on a perforated plate

A perforated SMA plate is subjected to tension displacement loading until it reaches a 7 % nominal strain. The stress-induced martensitic transformation of this plate and the accompanying localization phenomenon are analyzed under plane-stress assumption. The dimensions of the plate and the model parameter values are given in Fig. 15. Firstly, initial symmetry conditions are retained during the simulation, assuming (hypothetically) that the ongoing phase transformation will not disturb this property. Hence, only 1/4 of the thin plate is modelled. Several values of the internal length parameter ℓ are tested ($\ell = 5$ mm, $\ell = 10$ mm and $\ell = 50$ mm).

Fig. 16 displays the evolution of the spatial distribution of the martensite nonlocal volume fraction along with loading for different values of the internal length parameter ℓ. It can be observed that for lower values of the internal

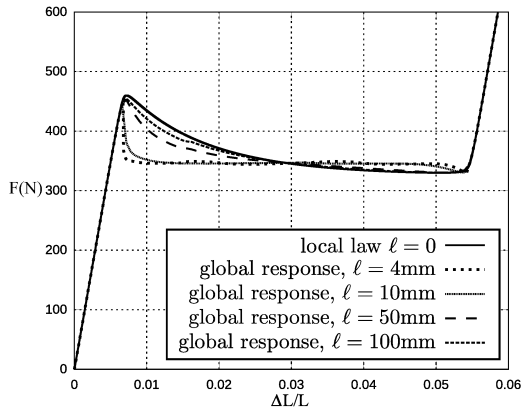

Figure 12: Influence of the internal length parameter ℓ on the force-displacement response.

length, transformation localization starts around the hole and continues under the form of a narrow band, before gradually fading (propagation) when saturation of the transformation is reached. For higher values of ℓ, Fig. 16 shows no localization of the phase transformation, this latter is homogeneous over the whole structure throughout the entire loading. Hence, the role of the hole in initiating localization is neutralized by a higher value of the internal length parameter.

The same problem is treated by relaxing the symmetry conditions. The distributions of martensitic volume fraction which are predicted by the developed model for different values of ℓ and at different loading stages are reported in Fig. 17. This latter shows more sparse martensitic transformation. Localizations are observed for lower values of the internal length parameter and earlier during loading compared to the symmetric configuration. The martensitic transformation annihilates the symmetry, which seems promoting the generalization of martensitic transformation over the whole domain.

The simulations presented above show the importance of two key parameters of the model $H_{\overline{f}}$ and ℓ. The first one controls the softening rate and the second one dictates the size of localization area. This latter is influenced by material and geometrical factors. The experimental identification of these parameters is an important feature of this modelling approach that needs to be improved.

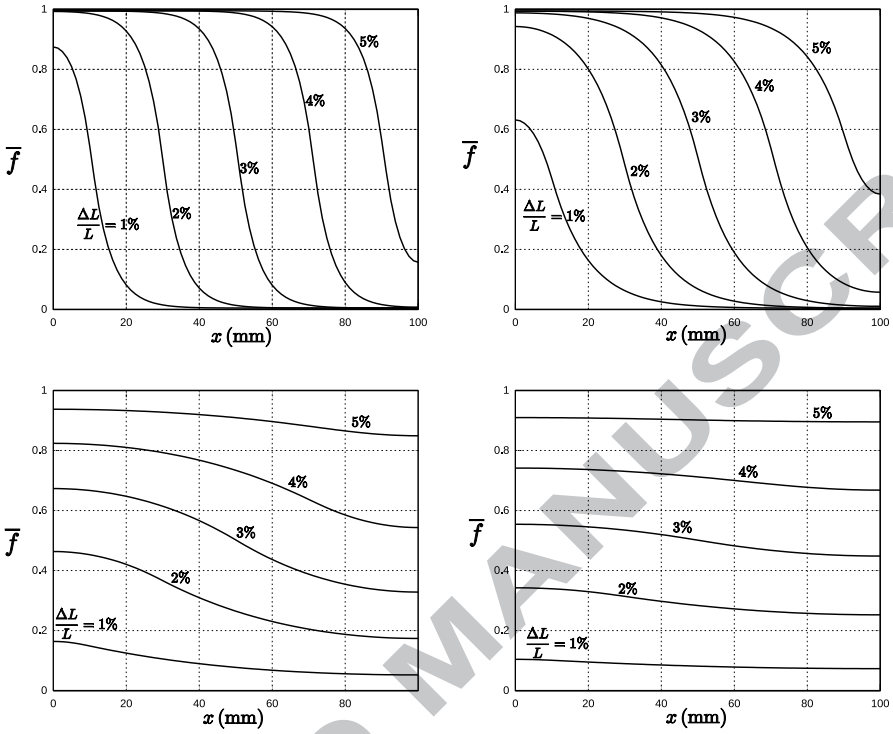

Figure 13: Distribution of nonlocal martensite volume fraction along the SMA wire at different loading steps, (a): $\ell = 4$ mm, (b): $\ell = 10$ mm, (c): $\ell = 50$ mm, (d): $\ell = 100$ mm.

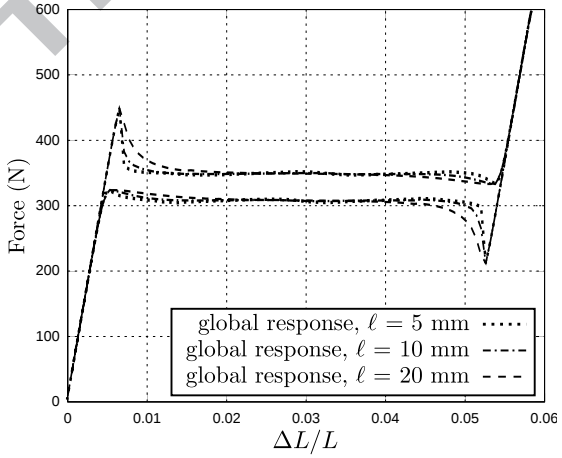

Figure 14: Force-displacement response of the SMA wire under tension loading/unloading for different values of the internal length parameter ℓ.

6. Conclusion

A nonlocal constitutive model which is based on the implicit gradient method is proposed for superelastic SMA materials. Its implementation in a finite element software (`Abaqus`®) necessitates the development of 1D and 2D standard C^0 finite elements with the nonlocal internal variable of phase transformation as an additional degree of freedom. The resulting numerical tool satisfactorily describes the localization of the martensite transformation and its front propagation in the case of SMA wire and film under mechanical loading. The nonlocal model is obtained as an extension of a recently proposed local model, that proves its efficiency in describing bulk SMA behavior. It involves only two additional parameters (ℓ and $H_{\overline{f}}$) which control the size of the localization zone and the softening rate.

The performed nonlocal analyses have been conducted for SMA wire and film undergoing martensite transformation under tension proportional loading (and unloading for the wire). The ability of the model to capture size effects and to reproduce SMA response such as hysteresis and internal loops under proportional and complex loading/unloading paths are under investigation. The present nonlocal approach will also be extended to the shape memory effect behavior. A particular key improvement will be the theoretical and experimental characterization of the material internal length parameter, that is *a priori* linked to the material grain size and geometrical factors.

A. Expressions of matrices $\left[\boldsymbol{B}_{\boldsymbol{N}}^{\overline{\boldsymbol{f}}}\right]$ and $\left[\boldsymbol{B}_{\boldsymbol{N}}^{\overline{\boldsymbol{f}}}\right]$

For a given point (ξ, η) in the reference element, the displacement vector $\overrightarrow{u}$ is expressed as a function of nodal displacements:

$$\overrightarrow{u}(\xi,\eta) = [N_N^u]\left\{u^N\right\} \tag{A.1}$$

with:

$$\left\{u^N\right\} = \begin{Bmatrix} u^1 \\ v^1 \\ u^2 \\ v^2 \\ u^3 \\ v^3 \\ u^4 \\ v^4 \end{Bmatrix} \quad \text{and} \quad \overrightarrow{u}(\xi,\eta) = \begin{Bmatrix} u(\xi,\eta) \\ v(\xi,\eta) \end{Bmatrix} \tag{A.2}$$

The interpolation matrix $[N_N^u]$ is given by:

$$[N_N^u(\xi,\eta)] = \begin{bmatrix} N_1 & 0 & N_2 & 0 & N_3 & 0 & N_4 & 0 \\ 0 & N_1 & 0 & N_2 & 0 & N_3 & 0 & N_4 \end{bmatrix} \tag{A.3}$$

where N_i are the shape functions:

$$\begin{aligned} N_1(\xi,\eta) &= \frac{(1-\xi)(1-\eta)}{4} \\ N_2(\xi,\eta) &= \frac{(1+\xi)(1-\eta)}{4} \\ N_3(\xi,\eta) &= \frac{(1+\xi)(1+\eta)}{4} \\ N_4(\xi,\eta) &= \frac{(1-\xi)(1+\eta)}{4} \end{aligned} \tag{A.4}$$

The strain vector is expressed from the displacement derivatives as:

$$\left\{ \begin{array}{c} E_{xx} \\ E_{yy} \\ 2E_{xy} \end{array} \right\} = \overbrace{\left[\begin{array}{cccc} 1 & 0 & 0 & 0 \\ 0 & 0 & 0 & 1 \\ 0 & 1 & 1 & 0 \end{array} \right]}^{[M^{str}]} \left\{ \begin{array}{c} u_{,x} \\ u_{,y} \\ v_{,x} \\ v_{,y} \end{array} \right\} \tag{A.5}$$

To express the displacement derivatives in the reference element, the following jacobian $[\mathcal{J}]$ is introduced:

$$\left\{ \begin{array}{c} \frac{\partial}{\partial \xi} \\ \frac{\partial}{\partial \eta} \end{array} \right\} = \left[\begin{array}{cc} \frac{\partial x}{\partial \xi} & \frac{\partial y}{\partial \xi} \\ \frac{\partial x}{\partial \eta} & \frac{\partial y}{\partial \eta} \end{array} \right] \left\{ \begin{array}{c} \frac{\partial}{\partial x} \\ \frac{\partial}{\partial y} \end{array} \right\} = [\mathcal{J}] \left\{ \begin{array}{c} \frac{\partial}{\partial x} \\ \frac{\partial}{\partial y} \end{array} \right\} \tag{A.6}$$

with the inverse relation:

$$\left\{ \begin{array}{c} \frac{\partial}{\partial x} \\ \frac{\partial}{\partial y} \end{array} \right\} = [\mathcal{J}]^{-1} \left\{ \begin{array}{c} \frac{\partial}{\partial \xi} \\ \frac{\partial}{\partial \eta} \end{array} \right\} \tag{A.7}$$

The jacobian is obtained from the shape functions and the nodal coordinates as follows:

$$[\mathcal{J}] = \left[\begin{array}{cccc} N_{1,\xi} & N_{2,\xi} & N_{3,\xi} & N_{4,\xi} \\ N_{1,\eta} & N_{2,\eta} & N_{3,\eta} & N_{4,\eta} \end{array} \right] \left[\begin{array}{cc} x^1 & y^1 \\ x^2 & y^2 \\ x^3 & y^3 \\ x^4 & y^4 \end{array} \right] \tag{A.8}$$

The transition from structural element to reference element is achieved by using the jacobian according to:

$$\left\{ \begin{array}{c} u_{,x} \\ u_{,y} \\ v_{,x} \\ v_{,y} \end{array} \right\} = \overbrace{\left[\begin{array}{cc} [\mathcal{J}]^{-1} & [0] \\ (0] & [\mathcal{J}]^{-1} \end{array} \right]}^{[M^{trans}]} \left\{ \begin{array}{c} u_{,\xi} \\ u_{,\eta} \\ v_{,\xi} \\ v_{,\eta} \end{array} \right\} \tag{A.9}$$

where the displacement derivatives with respect to the reference variables are given by:

$$\left\{\begin{array}{c} u_{,\xi} \\ u_{,\eta} \\ v_{,\xi} \\ v_{,\eta} \end{array}\right\} = \overbrace{\left[\begin{array}{cccccccc} N_{1,\xi} & 0 & N_{2,\xi} & 0 & N_{3,\xi} & 0 & N_{4,\xi} & 0 \\ N_{1,\eta} & 0 & N_{2,\eta} & 0 & N_{3,\eta} & 0 & N_{4,\eta} & 0 \\ 0 & N_{1,\xi} & 0 & N_{2,\xi} & 0 & N_{3,\xi} & 0 & N_{4,\xi} \\ 0 & N_{1,\eta} & 0 & N_{2,\eta} & 0 & N_{3,\eta} & 0 & N_{4,\eta} \end{array}\right]}^{[M^{grad}]} \left\{\begin{array}{c} u^1 \\ v^1 \\ u^2 \\ v^2 \\ u^3 \\ v^3 \\ u^4 \\ v^4 \end{array}\right\} \tag{A.10}$$

Finally, the matrix $[B_N^u]$ linking the strain vector to the nodal displacements is defined by:

$$\{E\} = [B_N^u]\left\{u^N\right\} = \left[M^{str}\right]\left[M^{trans}\right]\left[M^{grad}\right]\left\{u^N\right\} \tag{A.11}$$

The same procedure is applied for the nonlocal martensite volume fraction. It is a function of the nodal nonlocal martensite volume fractions,

$$\left\{\overline{f}\right\} = \left\{\begin{array}{c} \overline{f}^1 \\ \overline{f}^2 \\ \overline{f}^3 \\ \overline{f}^4 \end{array}\right\} \tag{A.12}$$

and the interpolation matrix,

$$\left[N_N^{\overline{f}}(\xi,\eta)\right] = \left[\begin{array}{cccc} N_1 & N_2 & N_3 & N_4 \end{array}\right] \tag{A.13}$$

through the relation,

$$\overline{f}\,(\xi,\eta) = \left[N_N^{\overline{f}}\right]\left\{\overline{f}^N\right\} \tag{A.14}$$

The gradient of nonlocal martensite volume fraction reduces to:

$$\left\{\begin{array}{c} \overline{f}_{,x} \\ \overline{f}_{,y} \end{array}\right\} = [\mathcal{J}]^{-1}\left[\begin{array}{cccc} N_{1,\xi} & N_{2,\xi} & N_{3,\xi} & N_{4,\xi} \\ N_{1,\eta} & N_{2,\eta} & N_{3,\eta} & N_{4,\eta} \end{array}\right]\left\{\begin{array}{c} \overline{f}^1 \\ \overline{f}^2 \\ \overline{f}^3 \\ \overline{f}^4 \end{array}\right\} = \left[B_N^{\overline{f}}\right]\left\{\overline{f}^N\right\} \tag{A.15}$$

References

Ahluwalia, R., Lookman, T., Saxena, A., Albers, R., 2004. Landau theory for shape memory polycrystals. Acta Materialia 52 (1), 209–218. 3

Arghavani, J., Auricchio, F., Naghdabadi, R., Reali, A., Sohrabpour, S., 2010. A 3-d phenomenological constitutive model for shape memory alloys under multiaxial loadings. International Journal of Plasticity 26 (7), 976 – 991. 2

Azadi, B., Rajapakse, R., Maijer, D., 2007. Multi-dimensional constitutive modeling of sma during unstable pseudoelastic behavior. International Journal of Solids and Structures 44 (20), 6473 – 6490. 2

Bekker, A., Brinson, L. C., 1998. Phase diagram based description of the hysteresis behavior of shape memory alloys. Acta Materialia 46 (10), 3649–3665. 2

Bellouard, Y., 2008. Shape memory alloys for microsystems: A review from a material research perspective. Materials Science and Engineering: A 481–482, 582–589. 2

Benard, W., Kahn, H., Heuer, A., Huff, M., 1998. Thin film shape memory alloy actuated micropumps. Journal of Microelectromechanical Systems 7, 145–251. 2

Cai, Z., Dai, H. H., 2006. Phase transitions in a slender cylinder composed of an incompressible elastic material. ii. analytical solutions for two boundary-value problems. Proceedings of the Royal Society A: Mathematical, Physical & Engineering Sciences 462, 419–438. 2

Chang, B., Shaw, J. A., Iadicola, M. A., 2006. Thermodynamics of shape memory alloy wire: modeling, experiments and application. Continuum Mech. Thermodyn. 18, 83–118. 2, 3

Churchill, C., Shaw, J., Iadicola, M., 2009. Tips and tricks for characterizing shape memory alloy wire: Part2 - Fundamental isothermal responses. Experimental Techniques 33, 51–62. 4, 5

Collard, C., Ben Zineb, T., Berbenni, S., Hardy, G., 2010. Simula+. `http://www.lpmm.fr/collard/simula+.html`. 18

Engelen, R., Geers, M., Baaijens, F., 2003. Nonlocal implicit gradient-enhanced elastoplasticity for the modelling of softening behaviour. International Journal of Plasticity 19, 403–433. 3, 9, 10, 11, 12

Grabe, C., Bruhns, O., 2009. Path dependence and multiaxial behavior of a polycrystalline NiTi alloy within the pseudoelastic and pseudoplastic temperature regimes. International Journal of Plasticity 25 (3), 513–545. 7

He, Y. J., Sun, Q. P., 2009a. Effects of structural and material length scales on stress-induced martensite macro-domain patterns in tube configurations. International Journal of Solids and Structures 46 (16), 3045–3060. 2, 10

He, Y. J., Sun, Q. P., 2009b. Scaling relationship on macroscopic helical domains in niti tubes. International Journal of Solids and Structures 46 (24), 4242–4251. 2, 10

He, Y. J., Sun, Q. P., 2010. Macroscopic equilibrium domain structure and geometric compatibility in elastic phase transition of thin plates. International Journal of Mechanical Sciences 52 (2), 198–211. 2, 10

Jirásek, M., Bažant, Z., 2002. Inelastic analysis of structures. Wiley, Ch. 26, pp. 517–539. 9, 10

Kyung, J., Ko, B., Ha, Y., Chung, G., 2008. Design of a microgripper for micromanipulation of microcomponents using sma wires and flexible hinges. Sensors and Actuators A 141 (1), 144–150. 2

Panico, M., Brinson, L. C., 2007. A three-dimensional phenomenological model for martensite reorientation in shape memory alloys. Journal of the Mechanics and Physics of Solids 55 (11), 2491–2511. 2

Peerlings, R., Geers, M., Borst, R. D., Brekelmans, W., 2001. A critical comparison of nonlocal and gradient-enhanced softening continua. International Journal of Solids and Structures 38 (44–45), 7723–7746. 3, 9, 10, 11, 12

Peultier, B., Ben Zineb, T., Patoor, E., 2006. Macroscopic constitutive law of shape memory alloy thermomechanical behaviour. Application to structure computation by FEM. Mechanics of Materials 38 (5-6), 510–524. 2, 3, 4, 6, 7, 9

Pijaudier-Cabot, G., Bažant, Z., 1987. Nonlocal damage theory. Journal of Engineering Mechanics-ASCE 113 (10), 1512–1533. 11

Popov, P., Lagoudas, D. C., 2007. A 3-D constitutive model for shape memory alloys incorporating pseudoelasticity and detwinning of self-accommodated martensite. International Journal of Plasticity 23 (10-11), 1679–1720. 2

Raniecki, B., Lexcellent, C., 1998. Thermodynamics of isotropic pseudoelasticity in shape memory alloys. European Journal of Mechanics - A/Solids 17 (2), 185–205. 2

Reynaerts, D., Peirs, J., Brussel, H. V., 1997. An implantable drug-delivery system based on shape memory alloy micro-actuation. Sensors and Actuators A 61 (1–3), 455–462. 2

Saint-Sulpice, L., Chirani, S. A., Calloch, S., 2009. A 3d super-elastic model for shape memory alloys taking into account progressive strain under cyclic loadings. Mechanics of Materials 41 (1), 12 – 26. 2

Shaw, J. A., Kyriakides, S., 1995. Thermomechanical aspects of NiTi. Journal of The Mechanics and Physics of Solids 43 (8), 1243–1281. 2, 13

Shaw, J. A., Kyriakides, S., 1997. On the nucleation and propagation of phase transformation fronts in a NiTi alloy. Acta Materialia 45 (2), 683–700. 2, 4

Shaw, J. A., Kyriakides, S., 1998. Initiation and propagation of localized deformation in elasto-plastic strips under uniaxial tension. International Journal of Plasticity 13 (10), 837–871. 2

Sittner, P., 2008. RoundRobin SMA modelling. `http://department.fzu.cz/ofm/wwwOFM/roundrobin`. 7, 19

Sun, Q., He, Y., 2008. A multiscale continuum model of the grain-size dependence of the stress hysteresis in shape memory alloy polycrystals. International Journal of Solids and Structures 45 (13), 3868–3896. 3, 4, 21

Tabib-Azar, M., Sutapun, B., Huff, M., 1999. Applications of TiNi thin films shape memory alloys in micro-opto-electro-mechanical systems. Sensors and Actuators 77 (1), 34–38. 2

Tanaka, K., 1986. A thermomechanical sketch of shape memory effect: One dimensional tensile behavior. Res Mechanica 18, 251–263. 2

Tanaka, K., Nishimura, F., Hayashi, T., Tobushi, H., Lexcellent, C., 1995. Phenomenological analysis on subloops and cyclic behavior in shape memory alloys under mechanical and/or thermal loads. Mechanics of Materials 19 (4), 281–292. 2

Thamburaja, P., 2005. Constitutive equations for martensitic reorientation and detwinning in shape-memory alloys. Journal of the Mechanics and Physics of Solids 53 (4), 825 – 856. 2

Truskinovsky, L., Vainchtein, A., 2004. The origin of nucleation peak in transformational plasticity. Journal of The Mechanics and Physics of Solids 52 (6), 1421–1446. 3

Zaki, W., Moumni, Z., 2007. A three-dimensional model of the thermomechanical behavior of shape memory alloys. Journal of the Mechanics and Physics of Solids 55 (11), 2455 – 2490. 2

Zauderer, E., 1989. Partial differential equations of applied mathematics, 2nd Edition. Wiley, Chichester, UK. 12

Table 1: Governing equations and parameters of the proposed model

Nonlocal internal variable definition:
$\overline{f}\left(\overrightarrow{x}\right) - \ell^2 \nabla^2 \overline{f}\left(\overrightarrow{x}\right) = f\left(\overrightarrow{x}\right)$
Transformation driving force:
$F_f = \bar{\varepsilon}^T_{sat} \Sigma_{eq} - B\left(T - T_0\right) - H_f f - \alpha_0 \frac{f-1}{f} - \alpha_1 \frac{f}{1-f}$
which verifies the condition,
$|F_f| \leq F_f^{crit}$
and reduces to:
$|F_f| = \left| \bar{\varepsilon}^T_{sat} \Sigma_{eq} - B\left(T - T_0\right) - H_f f - \alpha_0 \frac{f-1}{f} - \alpha_1 \frac{f}{1-f} \right| = F_f^{crit}$
during martensitic transformation.
Mechanical driving force:
$$E_{ij} = S_{ijkl} \Sigma_{kl} + \frac{3}{2} \frac{\Sigma^D_{ij}}{\Sigma_{eq}}$$
They will be solved by finite elements in conjunction with the **equilibrium equations**:
$\overrightarrow{\nabla} . \mathbf{\Sigma}\left(\overrightarrow{x}\right) = 0$
The following appropriate **boundary conditions** accompany the equations above:
$\overrightarrow{\nabla} \overline{f} = 0 \ \text{ on} \, \Gamma$
$\Sigma_{ij} n_j = T_i^u \ \text{ on} \, \Gamma^t$
$u_i = u_i^0 \ \text{ on} \, \Gamma^u$
Model parameters:
ℓ : internal length parameter (mm)
B : related to the transformation slope in the (Σ, T) diagram (MPa/°C)
T_0 : equilibrium temperature of phase transformation (°C)
$F_{f_0}^{crit}$: critical value of driving force at the beginning of phase transformation
H_f : transformation pseudo-hardening parameter (MPa)
$H_{\overline{f}}$: parameter controlling the softening rate
Y : Young modulus (MPa)
ε^T_{SAT} : saturation value of transformation strain
α_0 : penalisation parameter to ensure that variable f is greater than 0
α_1 : penalisation parameter to ensure that variable f is lower than 1

Point	ξ_i	η_i	ω_i
1	$-1/\sqrt{3}$	$-1/\sqrt{3}$	1
2	$1/\sqrt{3}$	$-1/\sqrt{3}$	1
3	$1/\sqrt{3}$	$1/\sqrt{3}$	1
4	$-1/\sqrt{3}$	$1/\sqrt{3}$	1

Table 2: Coordinates of Gauss points in the reference element.

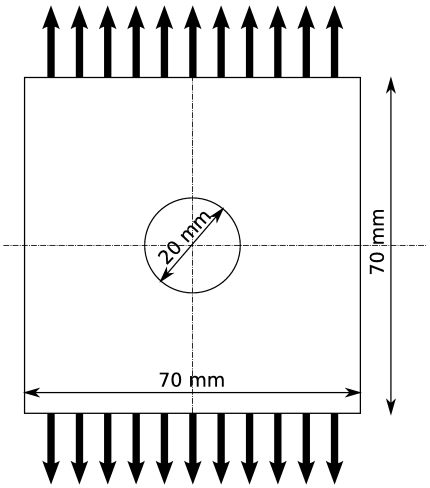

B	5 MPa/^{o}C
T	25 ^{o}C
T_0	-40 ^{o}C
$F_{f_0}^{crit}$	150 MPa
H_f	1 MPa
$H_{\overline{f}}$	1
Y	70 000 MPa
ε_{SAT}^{T}	0.05
α_0	0.1MPa
α_1	0.1MPa

Figure 15: Tensile test on a holed plate and material parameters.

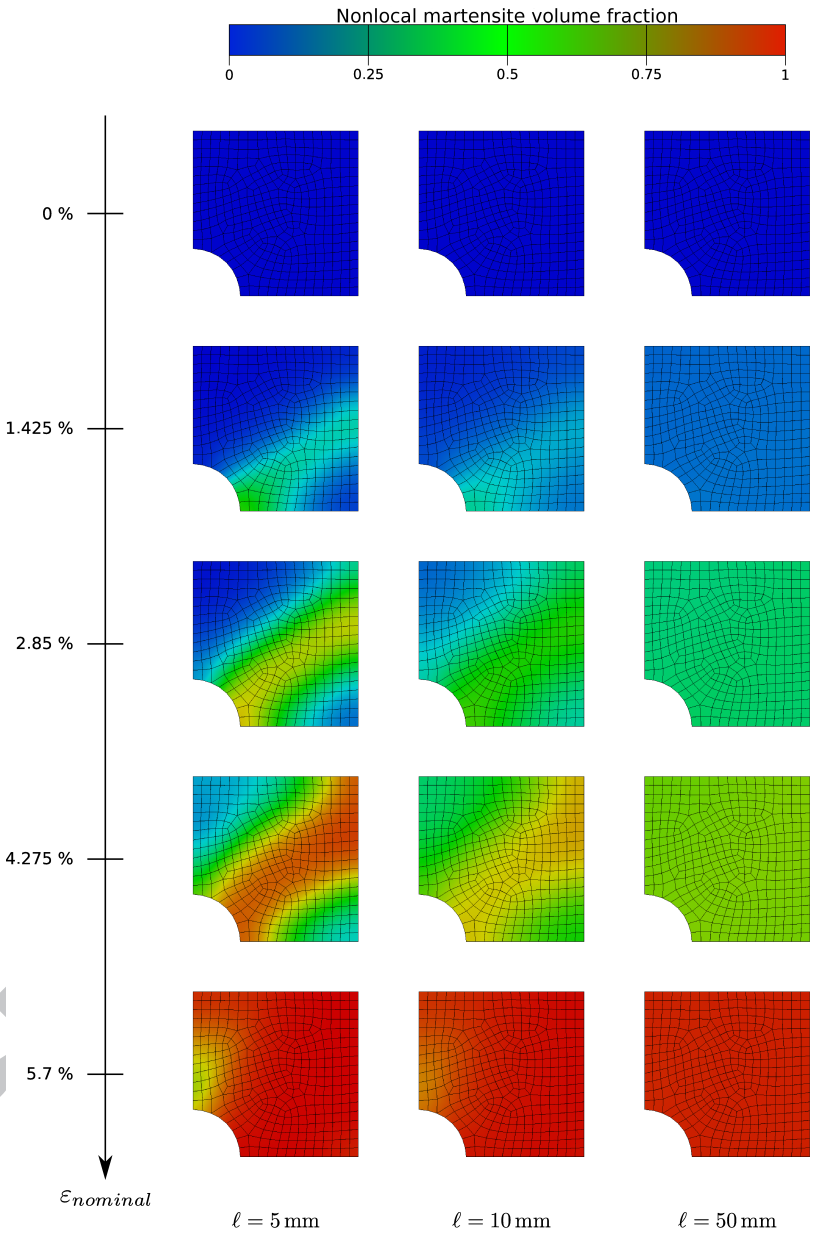

Figure 16: Spatial distributions of the nonlocal martensite volume fraction in an SMA holed thin plate under tension loading with symmetry conditions for different values of the internal length parameter.

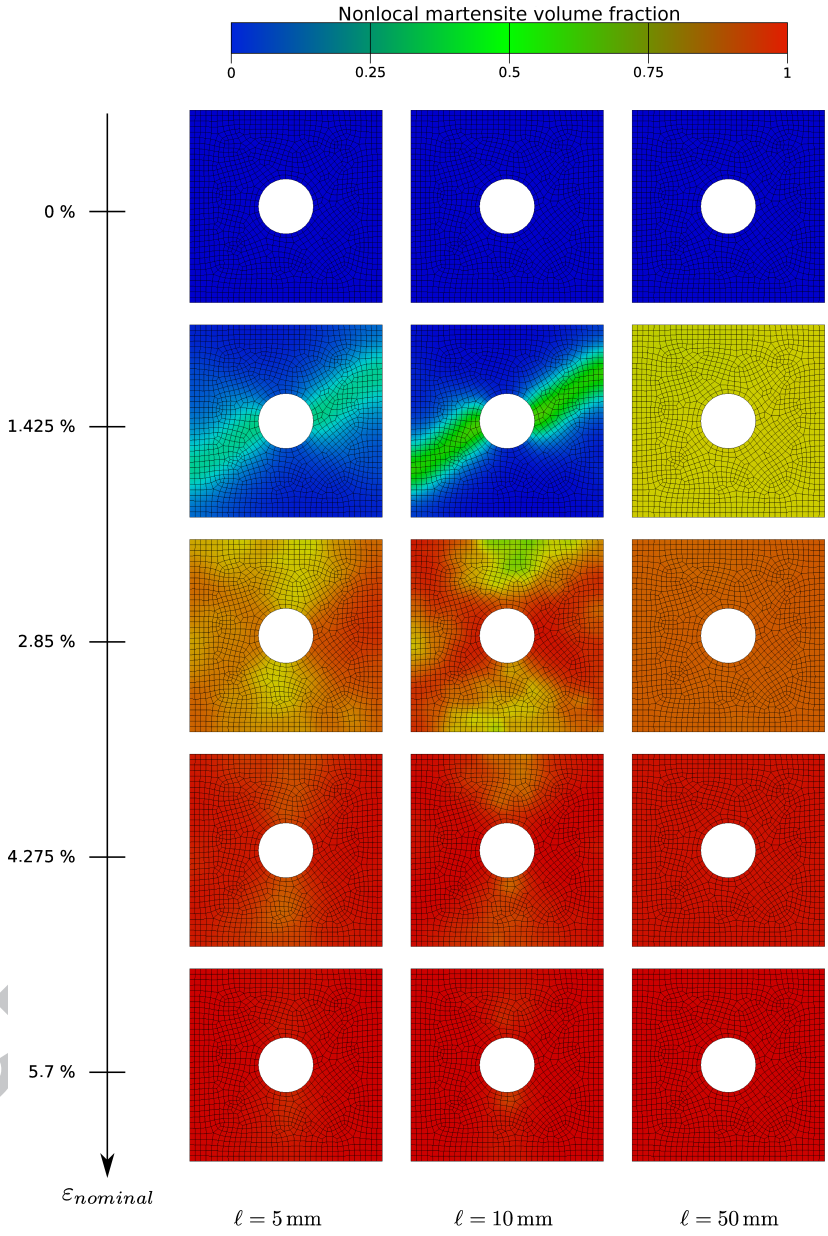

Figure 17: Spatial distributions of the nonlocal martensite volume fraction in an SMA holed thin plate under tension loading without symmetry conditions for different values of the internal length parameter.